Dalton Transactions

COMMUNICATION

View Article Online
View Journal | View Issue

Cite this: *Dalton Trans.*, 2014, **43**, 6623

Received 8th December 2013,
Accepted 7th February 2014

DOI: 10.1039/c3dt53450b

www.rsc.org/dalton

Bilayer stabilized Ln^{3+}-doped $CaMoO_4$ nanocrystals with high luminescence quantum efficiency and photocatalytic properties†

Chanchal Hazra, Tuhin Samanta, Aswin Vijai Asaithambi and Venkataramanan Mahalingam*

In this article, we discuss the microwave synthesis of sodium dodecyl sulphate (SDS) stabilized Ln^{3+}-doped $CaMoO_4$ nanocrystals (Ln^{3+} = Eu^{3+}, Er^{3+}/Yb^{3+}). The nanocrystals are quite monodispersed with an average size close to 100 nm. FTIR and TGA analyses suggest strong binding of the SDS molecules to the $CaMoO_4$ nanocrystals surface. The high dispersibility of the nanocrystals in water implies that SDS stabilizes the nanocrystals as a bilayer structure. The SDS coating also assists in the easy dispersion of the nanocrystals in toluene without any additional surface chemistry. The Eu^{3+} ions doped in the $CaMoO_4$ nanocrystals display very strong red luminescence with a quantum yield close to 40%. Under 980 nm excitation, Er^{3+}/Yb^{3+}-doped $CaMoO_4$ nanocrystals display Er^{3+} emissions at 550 and 650 nm. In addition, interestingly, a NIR peak at around 833 nm is observed, which occurred *via* a three photon process. Furthermore, the $CaMoO_4$ nanocrystals exhibit photocatalytic activity which is studied through the degradation of Rhodamine B (RhB) dye in neutral conditions. The RhB dye is significantly degraded by ~80% under UV illumination within 4 h and the rate of degradation is comparable to that observed for well known ZnO nanoparticles. The high luminescence quantum efficiency and strong photocatalytic activity of the Ln^{3+}-doped $CaMoO_4$ nanocrystals make them a potential material for dual applications such as bio-imaging and photocatalysis.

1. Introduction

Lanthanide (Ln^{3+})-doped luminescent nanomaterials continuously draw much attention due to their characteristic sharp transitions arising from inner 4f orbitals. The sharp transition is due to shielding of the 4f orbitals by the 5s and 5p orbitals.[1] These transitions have low absorption coefficients as they are partially forbidden, resulting in the long luminescence lifetime from the μs to ms region.[2] Intra 4f transitions are narrow and occur over a wide spectral region (from ultraviolet to near infrared) and give potential advantages for use in colour displays due to their high colour purity, phosphors, and biomarking applications.[3] In addition to the Stokes emission, these Ln^{3+} ions possess several energy levels which are close enough to convert the lower energy radiation to higher energy visible emission, a process known as upconversion luminescence.[4]

Recently there has been an increasing demand for water dispersible Ln^{3+}-doped nanocrystals due to their potential use as bioprobes.[5] Most of the studies in this area are mainly focussed towards developing Ln^{3+}-doped fluoride nanocrystals, partly due to their ease of synthesis as well as the availability of a range of synthetic procedures.[6–8] However, studies on water dispersible oxide-based materials, such as oxides, vanadates, phosphates, sulphates, and molybdates, are quite limited.[9] Oxide-based nanomaterials are interesting because of their robustness and lower toxicity.[10] Among the various Ln^{3+}-doped oxide nanomaterials, water dispersible molybdates are less explored. The molybdate (MoO_4^{2-}) crystal has tetrahedral symmetry (Td) with the central Mo^{2+} metal ion coordinated by four O^{2-} ions. As an interesting inorganic functional material, molybdates have attracted special attention because of their wide use in catalysis, luminescent materials, pigments, and so on.[11–16] Molybdate phosphors have broad and intense absorption bands due to charge transfer (CT) from oxygen to metal in the near-UV region.[17–21] For example, trivalent rare earth molybdate phosphors, such as $Y_2(MoO_4)_3$:Eu^{3+} and $Gd_2(MoO_4)_3$:Dy^{3+}, have been investigated because they are good hosts for red and green emitting phosphors for solid-state lighting based on InGaN diodes.[22–27] Not only Ln-based molybdates but alkali metal molybdates[28–31] are interesting due to the ionic size of the alkali metals being close to Ln^{3+} ions. Among the $MMoO_4$ (M = Ca^{2+}, Ba^{2+} & Sr^{2+}) materials, $CaMoO_4$ is attractive for the following reasons. First, $CaMoO_4$ is a highly

Department of Chemical Sciences, Indian Institute of Science Education and Research (IISER), Kolkata Mohanpur, West Bengal 741252, India.
E-mail: mvenkataramanan@yahoo.com; Fax: +91-33-25873020;
Tel: +91 (0)9007603474

†Electronic supplementary information (ESI) available: SEM, DLS, TGA, PL in toluene, solid state PL, life time, quantum yield, UC of $CaMoO_4$:Er^{3+} and $CaMoO_4$:Yb^{3+} NCs, UC power dependence study, pie chart diagram and photocatalysis kinetics. See DOI: 10.1039/c3dt53450b

transparent material which allows a wide range of light to pass through without much attenuation in luminescence. Second, $CaMoO_4$ is a robust phosphor due to its high density (4.25 g cm^{-3}) and possess better physical and chemical properties compared to other oxide materials. There have been quite a few reports on the Stokes luminescence of Ln^{3+}-doped $CaMoO_4$ nanocrystals in recent years.[32–36] Ju *et al.* have reported the synthesis of a $CaMoO_4$:Eu^{3+} phosphor *via* the sol–gel process. The quantum efficiency of this material is 20% higher than the one from a solid state reaction.[37] Sharma *et al.* have achieved a series of $CaMoO_4$ phosphors doped with Dy^{3+} and co-doped with K^+ by a hydrothermal method. They have performed photometric characterization of these nanocrystals which indicates the suitability of these phosphors in commercial white LEDs and other display devices.[38] Apart from Stokes luminescence, there are some reports available on the upconversion luminescence of Ln^{3+}-doped $CaMoO_4$ nanomaterials.[39] Ryu *et al.* have reported controllable white upconversion luminescence in Ho^{3+}/Yb^{3+}/Tm^{3+}-doped $CaMoO_4$ nanocrystals synthesized using a complex citrate-gel method.[40] The same group has shown green upconversion luminescence from polycrystalline Er^{3+}/Yb^{3+}-co-doped $CaMoO_4$ nanocrystals and also the effect of Li^+ doping on the enhancement of the green UC emission.[41] However, most of these reports discuss solid state materials. To fully explore the potential application of molybdates, it would be highly desirable to downscale their sizes to the nanoregime to expand their potential for various applications.

In this article, we report the synthesis of water dispersible Eu^{3+}-doped $CaMoO_4$ nanocrystals under microwave conditions. The water dispersibility is achieved with a thin coating of sodium dodecyl sulphate (SDS) over the Ln^{3+}-doped $CaMoO_4$ surface. The optimum concentration of Eu^{3+} is 5 mol%, leading to a very intense luminescence signal in water. This led to an enhanced Eu^{3+} luminescence quantum efficiency close to 40% in the $CaMoO_4$ nanocrystals. Under 980 excitation, Er^{3+}/Yb^{3+}-doped $CaMoO_4$ nanocrystals show a strong peak close to 833 nm in the NIR region, which, to our knowledge, is rarely reported.[42] Furthermore, the nanocrystals display strong photocatalytic activity which is verified through the degradation of Rhodamine B (RhB) dye. We observed an 80% degradation of RhB under UV illumination, which is close to that reported for ZnO. The high luminescence quantum efficiency and strong photocatalytic properties of the Ln^{3+}-doped $CaMoO_4$ nanocrystals make them suitable materials for dual applications.

2. Experimental section

2.1 Materials

Eu_2O_3, Er_2O_3, Yb_2O_3 (from Sigma-Aldrich), ammonium heptamolybdate tetrahydrate [$(NH_4)_6Mo_7O_{24}\cdot4H_2O$], $CaCl_2$ (from Merck), deionized water, 1 (M) HNO_3 (Merck, 70% pure), sodium dodecyl sulphate (SDS) were purchased from Merck. All the chemicals were used without further purification.

2.2 Synthesis

Water dispersible Eu^{3+}-doped $CaMoO_4$ nanocrystals were synthesized using a microwave (MW) procedure. Briefly, stoichiometric amounts of Eu_2O_3 were converted into their corresponding nitrates by dissolving in 1 M HNO_3 whereas $CaCl_2$, $(NH_4)_6Mo_7O_{24}\cdot4H_2O$ and SDS were used as received. In a typical procedure, a $(NH_4)_6Mo_7O_{24}\cdot4H_2O$–$H_2O$ stock solution was prepared by dissolving 1 mmol $(NH_4)_6Mo_7O_{24}\cdot4H_2O$ in 25 ml H_2O at room temperature. A mixture of $CaCl_2$ (0.95 mmol, 105.44 mg), $Eu(NO_3)_3$ (0.05 mmol, 16.9 mg), SDS (1 mmol, 288.38 mg) and 15 ml H_2O was heated to about 60 °C under vigorous stirring, forming a transparent solution. 2 ml from the $(NH_4)_6Mo_7O_{24}\cdot4H_2O$–$H_2O$ stock solution was slowly added into the mixture and the stirring was continued for another 10 min. Subsequently, the transparent solution was transferred to a 10 ml vial used for microwave synthesis and placed in the microwave reactor (Anton Paar Monowave 300). The vial was tightly sealed with a Teflon cap and then microwave heated at 90 °C for 10 minutes. Finally, the white coloured product appeared as a precipitate and was collected by centrifugation and washed three times with ethanol followed by deionized water to remove any unreacted reactants. For Er^{3+}/Yb^{3+}-doped $CaMoO_4$, the same protocol was followed, except $Er(NO_3)_3$ and $Yb(NO_3)_3$ were used instead of $Eu(NO_3)_3$.

2.3 Characterization

The XRD patterns were collected using a Rigaku-SmartLab diffractometer attached with a D/tex ultra detector and Cu K_α source operating at 35 mA and 70 kV. The scan range was set from 10–70° 2θ with a step size of 0.02° and a count time of 2 s. The samples were well powdered and spread evenly on a quartz slide. Field emission scanning electron microscopy (FESEM) images were taken on a SUPRA 55-VP instrument with patented GEMINI column technology. Prior to loading the samples into the chamber, they were coated with a thin film of gold–palladium in order to avoid charging effects. TEM images were taken on a UHR-FEG-TEM, JEOL; JEM 2100 F model using a 200 kV electron source. The samples were prepared by placing a drop of an aqueous dispersion of the nanocrystals on a carbon coated copper grid and the grid was dried in air. Thermogravimetric analysis was performed using a Mettler Toledo TGA 851 instrument under a N_2 atmosphere at a heating rate of 10° min^{-1}. Room temperature optical absorption spectra of all the samples were recorded on a Hitachi U4100 spectrophotometer. The samples were taken in a 3 ml quartz cuvette (path length, 1 cm). The PL spectra were measured on a Horiba Jobin Yvon spectrometer equipped with a 450 W Xe lamp. The excitation and emission light was dispersed using a Czerny-Turner monochromator with an optical resolution of 1 nm. The emitted photons were detected using a Hamamatsu R928 detector. The output signal was recorded using a computer. For the upconversion measurements, the nanocrystal dispersion was excited with a 980 nm diode laser from a RgBLase LLC, which was coupled with a fibre with a core diameter of 100 μm. The output signal was measured

using a Jobin Yvon spectrometer. The PL lifetime measurements were performed with a Horiba Jobin Yvon Fluorolog CP machine equipped with a pulsed Xe source operating at 25 W.

3. Results and discussion

The microwave method used for the synthesis of SDS-capped Ln^{3+}-doped $CaMoO_4$ [Ln^{3+} = Eu^{3+}, Er^{3+}/Yb^{3+}] nanocrystals led to the formation of water dispersible nanocrystals in the size range of 100 nm. The high water dispersibility suggests that the SDS coating is in the form of a bilayer. This is confirmed from the luminescence studies (*vide infra*). These nanocrystals are quite monodisperse and spherical in shape, as confirmed from the HR-TEM image shown in Fig. 1. The high monodispersity in the size is further substantiated by the narrow distribution obtained with DLS measurements (Fig. 1B). The hydrodynamic size of the nanocrystals obtained from the DLS measurements is about 120 nm. This is also supported by the SEM images shown in Fig. S1 in the ESI.† The formation of pure tetragonal phase $CaMoO_4$ nanocrystals is verified from the XRD patterns shown in Fig. 2. The observed diffraction peaks match very well with the standard pattern of tetragonal phase $CaMoO_4$ (ICSD PDF card no: 01-085-1267).

The strong diffraction peaks clearly indicate good crystallinity in the as-synthesized products. The absence of any additional peaks suggests that $CaMoO_4$ nanocrystals with high phase purity can be easily obtained through a microwave synthetic method. The binding of SDS molecules to the surface of the $CaMoO_4$ nanocrystals is confirmed by the FTIR spectra shown in Fig. 3. Briefly, a broad band centered at 3350 cm^{-1} due to O–H stretching vibrations is observed. The C–H stretching vibrations of the methylene ($-CH_2$) units are observed near 2850 cm^{-1} and 2922 cm^{-1}. The region between 600 to 900 cm^{-1} indicates C–H bending frequencies of $-CH_2$ units. For the pure SDS, two strong peaks are noted near 1090 cm^{-1} (symmetric stretching) and 1225 cm^{-1} (asymmetric stretching), which are assigned to the S=O groups of sulphate. These peaks shift to lower energy and merge in the case of the SDS coated nanocrystals, indicating the binding of the S=O groups of SDS to the nanocrystals. To further confirm the SDS coating on the surface of the $CaMoO_4$ nanocrystals, TGA analysis was conducted. The TGA curves for SDS coated $CaMoO_4$ and the free SDS are compared in Fig. S2 in the ESI.† For the free SDS, the major weight loss is from 168 to 350 °C due to the decomposition of the SDS molecules. For the SDS coated $CaMoO_4$ nanocrystals, the onset of decomposition is shifted to a higher temperature (220 °C). This substantiates the FTIR results that the SDS molecules are attached strongly to the $CaMoO_4$ surface. In addition, the narrow decomposition range indicates that all the nanocrystals are more or less evenly coated with the SDS. Optical studies of the SDS coated Eu^{3+}-doped $CaMoO_4$ nanocrystals show some interesting characteristics. Upon UV (394 nm) excitation, the nanocrystals emit strong emission near 614 nm, as shown in Fig. 4, which is assigned to a $^5D_0 \rightarrow {}^7F_2$ transition. In addition to the strong emission at 614 nm, there are less intense emission peaks observed near 590, 650 and 700 nm. These peaks are respectively ascribed to $^5D_0 \rightarrow {}^7F_1$, $^5D_0 \rightarrow {}^7F_3$ and $^5D_0 \rightarrow {}^7F_4$ transitions. The $^5D_0 \rightarrow {}^7F_2$ transition, being quite intense, gives rise to bright red light from a 0.1 wt% aqueous dispersion of the Eu^{3+}-doped $CaMoO_4$ nanocrystals (shown in the inset of Fig. 4). The $^5D_0 \rightarrow {}^7F_2$ emission is hypersensitive in nature and its intensity depends on the local crystallite environment around the Ln^{3+} ions. An intense $^5D_0 \rightarrow {}^7F_2$ transition is generally

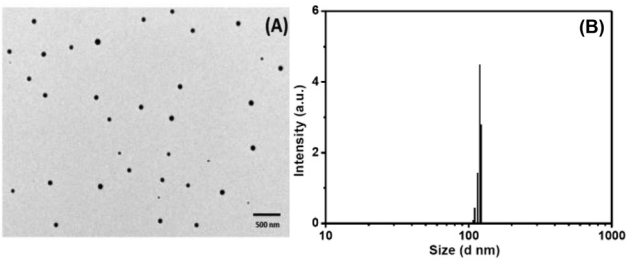

Fig. 1 TEM image (A) and particle size distribution from DLS (B) of the water dispersed $CaMoO_4$:Eu^{3+} nanocrystals, indicating the formation of monodispersed nanocrystals.

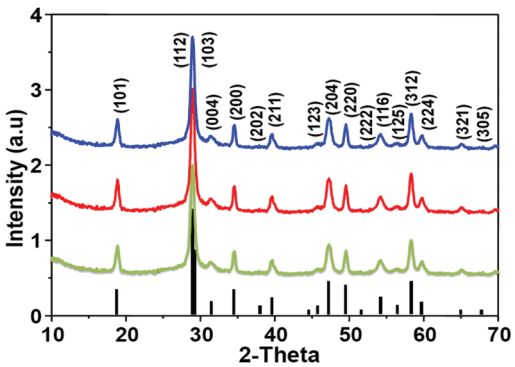

Fig. 2 XRD patterns of the $CaMoO_4$ nanocrystals: (green) undoped, (red) Eu^{3+}-doped and (blue) Er^{3+}/Yb^{3+}-doped and the standard pattern (black).

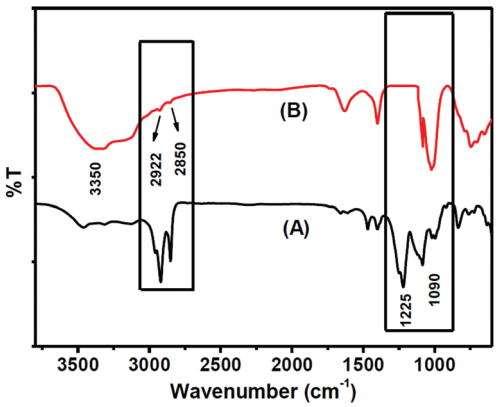

Fig. 3 FTIR spectra of (A) the free SDS molecules, (B) the SDS capped nanocrystals in H_2O.

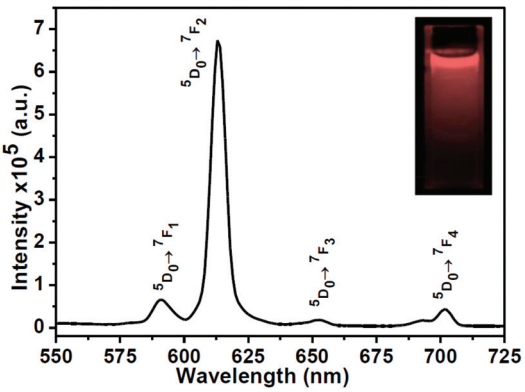

Fig. 4 Emission spectrum of the SDS coated 0.1 wt% Eu^{3+}-doped $CaMoO_4$ nanocrystals in water. The inset shows a digital image of the colloidal nanocrystals under 366 nm UV light.

observed when Eu^{3+} ions are present in a non-centrosymmetric environment. However, in $CaMoO_4$, both Ca^{2+} and Mo^{2+} have S_4 point symmetry possessing an inversion centre. This suggests a weaker emission intensity for the $^5D_0 \rightarrow {}^7F_2$ transition. We believe that the observed strong emission might be due to the nanocrystals possessing some defects or disorder, leading to distortion in the symmetry sites where the Eu^{3+} ions occupy. This is verified by preparing bulk Eu^{3+}-doped $CaMoO_4$ nanocrystals *via* a sol–gel process. The material is heated at 800 °C to achieve better crystallinity. For the bulk powder sample, the asymmetric ratio (614/591) is 1.75 whereas for the SDS coated nanocrystals, the corresponding value is 7.75, suggesting more distortions near the crystal sites of Eu^{3+} in the case of the nanocrystals. The luminescence spectrum of the bulk material is shown in Fig. S3 in the ESI.† On the other hand, we believe there can be an alternative reason, such as a polarization effect, which alters the crystal field strength as well as affecting the transition probabilities.[36a,43]

The luminescence lifetime of the $^5D_0$ state of the Eu^{3+} ions in the SDS coated $CaMoO_4$:Eu^{3+}-doped nanocrystals is about 2.16 ms, as calculated from the decay analysis (shown in Fig. S4, ESI†). The intense luminescence signal and longer lifetime of the Eu^{3+} ions in the $CaMoO_4$:Eu^{3+}-doped nanocrystals is further supported by the quantum efficiency of the nanocrystals in an aqueous medium. The calculated quantum yield is about 40%, which is measured using quinine sulphate as the reference standard. The details of the measurement and the calculations are given in Fig. S5 in the ESI.† This value is higher than the calculated value of 15% for YVO_4:Eu^{3+} (5%) colloidal nanocrystals.[44] Haase *et al.* reported a luminescence quantum yield equal to 38% for colloidal YVO_4:Eu^{3+} (15%) nanocrystals with an average size of 30 nm at room temperature.[45] The above points clearly suggest that the SDS coated $CaMoO_4$:Eu^{3+} (5%) nanocrystals are a better matrix for Eu^{3+} ions. To our knowledge, there are very few reports with a high quantum yield for Eu^{3+} ion in water. To understand the reason for the increased quantum efficiency for Eu^{3+} ions in $CaMoO_4$ nanocrystals, we prepared Eu^{3+}-doped $CaMoO_4$ nanocrystals without the SDS coating under identical conditions. The observed lifetime for the Eu^{3+} ions is 1.93 ms, which is lower compared to the SDS coated $CaMoO_4$ nanocrystals (Fig. S6, ESI†). This implies that one of the reasons for the enhanced quantum efficiency for the Eu^{3+} ions in the $CaMoO_4$ matrix is the strong SDS coating, which can probably reduce the number of defects near the surface of the nanocrystals.

The high water dispersibility of the nanocrystals after SDS coating suggests that SDS is mostly in the form of a bilayer, and thus SO_3^- is on the surface of the nanocrystals. The bilayer formation is further verified by the slow addition of toluene to the water dispersible nanocrystals, which upon slight sonication led to the nanocrystals moving to the toluene phase. This phase transfer is supported by the strong Eu^{3+} emission from the nanocrystals dispersed in toluene (shown in Fig. S7, ESI†). It is interesting that the nanocrystals can be used both in organic and aqueous phases without additional surface chemistry.

The luminescence studies were extended to understand the upconversion ability of the $CaMoO_4$ nanocrystals by doping with Er^{3+}/Yb^{3+} ions. Due to their high absorption coefficient, Yb^{3+} ions are used as a sensitizer in the upconversion process. Moreover, it has only one excited electronic state ($^2F_{5/2}$) which matches with the 980 excitation wavelength. The nanocrystals in H_2O showed a weak emission whereas in toluene they exhibit an intense upconversion emission, which is shown in Fig. 5. The green emission peaks centered at 530 and 550 nm are assigned to the $^2H_{11/2} \rightarrow {}^4I_{15/2}$ and $^4S_{3/2} \rightarrow {}^4I_{15/2}$ transitions, respectively.

The other emission peak at 668 nm is assigned to the $^4F_{9/2} \rightarrow {}^4I_{15/2}$ transition. It is interesting to note that along with the characteristic green and red emission peaks, the nanocrystals exhibit a relatively strong peak close to 833 nm in the NIR region. This peak is assigned to the $^4I_{9/2} \rightarrow {}^4I_{15/2}$ transition. To the best of our knowledge, this NIR emission peak is less reported in the literature. To investigate the origin of this peak, we prepared $CaMoO_4$ nanocrystals doped with Er^{3+} and

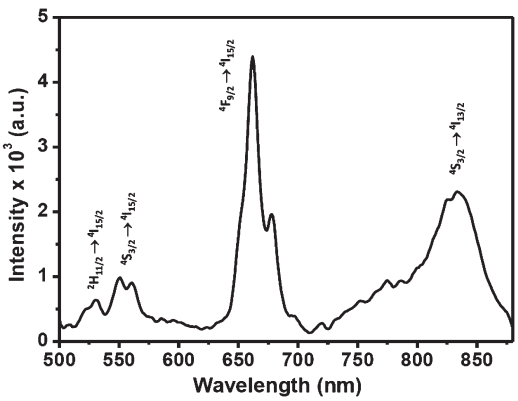

Fig. 5 Upconversion emission spectrum of the SDS coated Er^{3+}/Yb^{3+}-doped $CaMoO_4$ nanocrystals in toluene, measured by exciting the sample with a 980 nm diode laser at a 400 mW laser power.

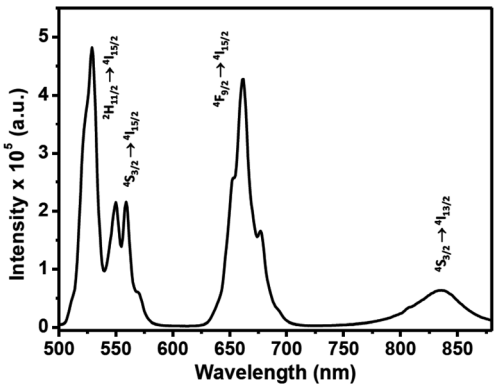

Fig. 6 Upconversion emission spectrum of the Er^{3+}/Yb^{3+}-doped $CaMoO_4$ nanocrystals (without the SDS coating), measured by exciting the sample with a 980 nm diode laser operating at a 400 mW laser power.

Yb^{3+} independently using a similar synthetic protocol. Hardly any emission was observed near 830 nm from both the samples upon exciting at 980 nm. These results suggest the absence of excited state absorption as well as scattering of light from the Yb^{3+} ions in the nanocrystals. The results are shown in Fig. S8 in the ESI.† To understand the mechanism responsible for the UC emission observed above, we prepared $CaMoO_4$:Yb^{3+}/Er^{3+} nanocrystals without the SDS coating. The UC emission spectrum of this sample, shown in Fig. 6, is quite different from that obtained with the SDS coated nanocrystals. A very strong green UC emission is observed for the nanocrystals prepared without the SDS coating. For the SDS-coated nanocrystals, the intensity ratio $I_{(NIR)}/I_{(red)}$ is about 1.40 whereas the corresponding value is only 0.38 for the nanocrystals without the SDS coating. These results suggest that the NIR emission is probably associated with surface properties of the nanocrystals. The number of photons involved in the energy transfer process is understood by conducting power dependent studies as the laser power, $P \alpha I^n$, where I is the intensity of the upconversion emission and n is the number of photons involved in generating the upconversion emission. A logarithmic plot of the laser power against the emission intensity gives a slope of n. As shown in Fig. S9 and S10 in the ESI,† the slopes (n) of the plots are 1.89 and 2.46 for the red and NIR emissions, respectively. Based on the above results, we propose the following mechanism, which is schematically shown in Fig. 7. First, Er^{3+} in the ground state is excited to $^4I_{11/2}$ *via* energy transfer (ET) from the Yb^{3+} ions. Because of the short lifetime of the $^4I_{11/2}$ state, most of the ions will non-radiatively decay and populate the $^4I_{13/2}$ state. The second energy transfer will excite the Er^{3+} ion and populate the $^4F_{9/2}$ state. The red emission occurs from this level. In addition, some of the excited Er^{3+} ions are excited higher in the energy to the $^2H_{9/2}$ state *via* the third energy transfer. Due to the presence of energy levels which are close enough, the excited Er^{3+} ions reach $^2H_{11/2}/^4S_{3/2}$ non-radiatively. We propose the following cross-relaxation ($^2H_{11/2}/^4S_{3/2}$, $^4I_{13/2}$)→($^4I_{9/2}$, $^4I_{9/2}$) occurs at this stage, thus populating the $^4I_{9/2}$ state. In the absence of such a cross-relaxation,

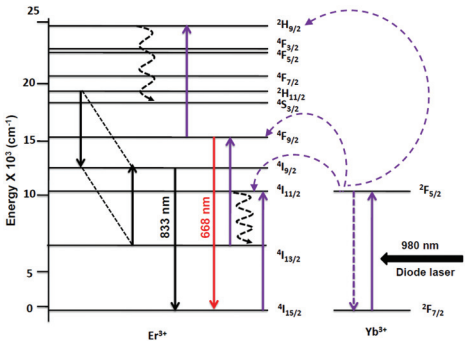

Fig. 7 Upconversion mechanism for the Er^{3+}/Yb^{3+}-doped $CaMoO_4$ nanocrystals prepared *via* a microwave method.

intense green emission occurs from the $^2H_{11/2}/^4S_{3/2}$ states. Though the reason for the cross-relaxation is not clear, we presume that the SDS ligands might have a role.

Finally, we have extended the study to investigate the photocatalytic activity of the $CaMoO_4$ nanocrystals. The photocatalytic activity of $PbMoO_4$ and $BiVO_4$ with a scheelite structure has been reported.[46,47] To the best of our knowledge, there is no report on the photocatalytic activity of $CaMoO_4$ nanocrystals. Because of the relatively high band gap energy of $CaMoO_4$ (E_g = 3.41 eV), the molybdate was tested as a photocatalyst under UV irradiation. The conduction band of $CaMoO_4$ is located above the RhB redox potential ($E^0_{RhB^{\bullet+}}$ = 1.34 eV) *versus* the standard calomel electrode (SCE), allowing CaMoO4 to be catalytically active. We believe that reactive oxygen species (*e.g.*, $HO^{\bullet}$, $O_2^{-\bullet}$, etc.), especially $HO^{\bullet}$ radicals, can oxidize the organic dye molecules and perform photocatalysis. The Rhodamine B (RhB) dye degradation was demonstrated over the surface of the $CaMoO_4$ nanocrystals under UV illumination to elucidate the photocatalytic activity. To ensure good adsorption of the dye onto the nanocrystals surface, the photocatalytic property was studied without the SDS coating. Fig. 8 shows that the RhB dye is significantly degraded by ~80% under UV illumination within 4 hours. The pie chart diagram of RhB dye degradation (see Fig. S11, ESI†) reveals

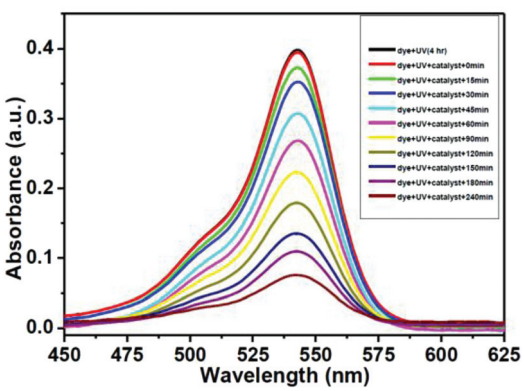

Fig. 8 UV-Vis spectra of RhB dye as a function of time over the $CaMoO_4$ nanocrystals.

that over half the concentration of the dye is degraded in the first 120 minutes.

The RhB dye degradation follows apparent first order kinetics, in agreement with a general Langmuir–Hinshelwood mechanism;

$$r = -\mathrm{d}C/\mathrm{d}t = k_1k_2C/1 + k_2C$$

where, r is the degradation rate of the dye (mg min^{-1}), C is the concentration of the dye (mg l^{-1}), t is the illumination time, k_2 is the adsorption coefficient of the dye (mg^{-1}), and k_1 is the reaction rate constant (mg min^{-1}). If C is very small then the above equation could be simplified to

$$\ln(C_0/C) = k_1k_2t = kt$$

where C_0 is the initial concentration of the dye, C is the concentration of the dye after a certain time t with UV illumination, k is the rate constant and t is the time. A plot of $\ln(C_0/C)$ *vs.* t (shown in Fig. S12, ESI†) provides a slope value of 0.0274 min^{-1}, which is nothing but the rate constant (k) of the dye degradation by the $CaMoO_4$ nanocrystals in the photocatalytic process. It is interesting to note that the resulting value is comparable with the reported value for a ZnO photocatalyst.[48]

4. Conclusions

In this article, we have reported the microwave synthesis of sodium dodecyl sulphate coated Ln^{3+}-doped $CaMoO_4$ nanocrystals (Ln^{3+} = Eu^{3+}, Er^{3+}/Yb^{3+}). SEM and TEM measurements suggest the average size of the nanocrystals to be 100 nm. FTIR and TGA analyses confirm that the SDS binds strongly to the nanocrystals. The high water dispersibility of the nanocrystals after the SDS coating suggests that the SDS coating is in the form of a bilayer. Upon UV excitation, the Eu^{3+}-doped $CaMoO_4$ nanocrystals show strong red emission, characteristic of Eu^{3+} ions, with a high quantum efficiency close to 40%. Under 980 nm excitation, the Er^{3+}/Yb^{3+}-doped $CaMoO_4$ nanocrystals exhibit upconversion luminescence in toluene. In addition, the nanocrystals show strong photocatalytic activity, which is verified from RhB dye degradation under UV illumination. The high quantum efficiency and water dispersibility of the Ln^{3+}-doped $CaMoO_4$ nanocrystals mean they can be used as potential materials for dual applications.

Acknowledgements

VM thanks the Department of Science and Technology (DST) India, CSIR and IISER-Kolkata for funding. CH and TS thank IISER-Kolkata and UGC respectively for their scholarships.

Notes and references

1 (*a*) A. J. Steckl, M. Garter, D. S. Lee, J. Heikenfeld and R. Birkhahn, *Appl. Phys. Lett.*, 1999, **75**, 2184; (*b*) J. H. Kim and P. H. Holloway, *Adv. Mater.*, 2005, **17**, 91.

2 (*a*) F. Auzel, *Chem. Rev.*, 2004, **104**, 139; (*b*) S. Sivakumar, F. C. J. M. van Veggel and M. Raudsepp, *J. Am. Chem. Soc.*, 2005, **127**, 12464; (*c*) S. Heer, O. Lehmann, M. Haase and H.-U. Güdel, *Angew. Chem., Int. Ed.*, 2003, **42**, 3179; (*d*) M. Haase and H. Schäfer, *Angew. Chem., Int. Ed.*, 2011, **50**, 5808; (*e*) F. Wang and X. Liu, *J. Am. Chem. Soc.*, 2008, **130**, 5642; (*f*) C. Li and J. Lin, *J. Mater. Chem.*, 2010, **20**, 6831; (*g*) S. Cotton, *Lanthanide and Actinide Chemistry*, John Wiley & Sons, West Sussex, 2006; (*h*) C. G. Bunzli, *Chem. Rev.*, 2002, **102**, 1897; (*i*) F. Wang, Y. Han, C. S. Lim, Y. Lu, J. Wang, J. Xu, H. Chen, C. Zhang, M. Hong and X. Liu, *Nature*, 2010, **463**, 1061; (*j*) V. Sudarsan, F. C. J. M. Van Veggel, R. A. Herring and M. Raudsepp, *J. Mater. Chem.*, 2005, **15**, 1332.

3 (*a*) G. Blasse and B. C. Grabmaier, *Luminescent Materials*, Springer, Berlin, 1994; (*b*) A. Kitai, *Luminescent Materials and Applications*, John Wiley & Sons, West Sussex, 2008; (*c*) C. R. Ronda, T. Justel and H. Nikol, *J. Alloys Compd.*, 1998, **275–277**, 669; (*d*) T. Montini, A. Speghini, L. De Rogatis, B. Lorenzut, M. Bettinelli, M. Graziani and P. Fornasiero, *J. Am. Chem. Soc.*, 2009, **131**, 13155.

4 (*a*) V. Mahalingam, M. Francesca, F. Vetrone, V. Venkatramu, A. Speghini, M. Bettinelli and J. A. Capobianco, *J. Phys. Chem. C*, 2008, **112**, 17745; (*b*) J. Silver, E. Barrett, P. J. Marsh and R. J. Withnall, *J. Phys. Chem. B*, 2003, **107**, 9236; (*c*) F. Pandozzi, F. Vetrone, J.-C. Boyer, R. Naccache, J. A. Capobianco, A. Speghini and M. A. Bettinelli, *J. Phys. Chem. B*, 2005, **109**, 17400; (*d*) J. Silver, M. I. Martinez-Rubio, T. G. Ireland, G. R. Fern and R. Withnall, *J. Phys. Chem. B*, 2001, **105**, 948; (*e*) H. Schafer, P. Ptacek, K. Kömpe and M. Haase, *Chem. Mater.*, 2007, **19**, 1396; (*f*) D. Chen, Y. Yu, F. Huang, P. Huang, A. Yang and Y. Wang, *J. Am. Chem. Soc.*, 2010, **132**, 9976; (*g*) X. Zhang, P. Yang, C. Li, D. Wang, J. Xu, S. Gai and J. Lin, *Chem. Commun.*, 2011, **47**, 12143; (*h*) N. J. J. Johnson, N. M. Sangeetha, J. C. Boyer and F. C. J. M. Van Veggel, *Nanoscale*, 2010, **2**, 771; (*i*) J. Pichaandi, F. C. J. M. Van Veggel and M. Raudsepp, *ACS Appl. Mater. Interfaces*, 2010, **2**, 157.

5 (*a*) D. E. Achatz, A. Rehamand and O. S. Wolfbeis, *Top. Curr. Chem.*, 2011, **300**, 29; (*b*) S. M. Saleh, R. Aliand and O. S. Wolfbeis, *Chem.–Eur. J.*, 2011, **17**, 14611; (*c*) N. Bogdan, E. M. Rodríguez, F. S. Rodríguez, M. C. I. de la Cruz, A. Juarranz, D. Jaque, J. G. Solé and J. A. Capobianco, *Nanoscale*, 2012, **4**, 3647; (*d*) G. Y. Chen, T. Y. Ohulchaskyy, W. Law, H. Agren and P. N. Prasad, *Nanoscale*, 2011, **3**, 2003; (*e*) S. Sarkar, C. Hazra, M. Chatti, V. Sudarsan and V. Mahalingam, *RSC Adv.*, 2012, **2**, 8269.

6 (*a*) H. Q. Wang and T. Nann, *ACS Nano*, 2009, **3**, 3804; (*b*) V. Mahalingam, F. Vetrone, R. Naccache, A. Speghini and J. A. Capobianco, *J. Mater. Chem.*, 2009, **19**, 3149; (*c*) S. Sarkar, C. Hazra and V. Mahalingam, *Dalton Trans.*, 2013, **42**, 63; (*d*) W. Quan, D. M. Yang, P. P. Yang, X. M. Zhang, H. Z. Lian, X. M. Liu and J. Lin, *Inorg. Chem.*, 2008, **47**, 9509; (*e*) S. Sarkar, C. Hazra and V. Mahalingam, *Chem.–Eur. J.*, 2012, **18**, 7054; (*f*) S. Sarkar,

B. Messaragandla, C. Hazra and V. Mahalingam, *Adv. Mater.*, 2013, **25**, 860; (*g*) P. Rahman and M. Green, *Nanoscale*, 2009, **1**, 214.

7 (*a*) G. Wang, Q. Peng and Y. Li, *Acc. Chem. Res.*, 2011, **44**, 322; (*b*) X. Yu, M. Li, M. Xie, L. Chen, Y. Li and Q. Wang, *Nano Res.*, 2010, **3**, 51; (*c*) F. Wang and X. Liu, *J. Am. Chem. Soc.*, 2008, **130**, 5642; (*d*) L. Wang, P. Li and Y. Li, *Adv. Mater.*, 2007, **19**, 3304; (*e*) C. Zhang, Z. Hou, R. Chai, Z. Cheng, Z. Xu, C. Li, L. Huangand and J. Lin, *J. Phys. Chem. C*, 2010, **114**, 6928; (*f*) H. P. Paudel, L. Zhong, K. Bayat, M. F. Baroughi, S. Smith, C. Lin, C. Jiang, M. Berry and S. May, *J. Phys. Chem. C*, 2011, **115**, 19028; (*g*) P. Ghosh, A. Kar and A. Patra, *J. Phys. Chem. C*, 2010, **114**, 715; (*h*) D. Yang, Y. Dai, P. Ma, X. Kang, M. Shang, Z. Cheng, C. Li and J. Lin, *J. Mater. Chem.*, 2012, **22**, 20618.

8 (*a*) S. Sarkar, C. Hazra and V. Mahalingam, *Dalton Trans.*, 2013, **42**, 63; (*b*) P. Ghosh, A. Kar and A. Patra, *Nanoscale*, 2010, **2**, 1196; (*c*) N. J. J. Johnson, A. Korinek, C. Dong and F. C. J. M. van Veggel, *J. Am. Chem. Soc.*, 2012, **134**, 11068; (*d*) N. J. J. Johnson and F. C. J. M. Van Veggel, *Nano Res.*, 2013, **6**, 547; (*e*) S. Li, X. Zhang, Z. Hou, Z. Cheng, P. Ma and J. Lin, *Nanoscale*, 2012, **4**, 5619; (*f*) X. Zhang, P. Yang, C. Li, D. Wang, J. Xu, S. Gai and J. Lin, *Chem. Commun.*, 2011, **47**, 12143; (*g*) C. Li, Z. Xu, D. Yang, Z. Cheng, Z. Hou, P. Ma, H. Lian and J. Lin, *CrystEngComm*, 2012, **14**, 670.

9 (*a*) H. Chen and J. Ren, *Analyst*, 2012, **137**, 1899; (*b*) C. Hazra and V. Mahalingam, *RSC Adv.*, 2013, **3**, 9197; (*c*) Y. C. Chen, Y. C. Wu, D. Y. Wang and T. M. Chen, *J. Mater. Chem.*, 2012, **22**, 7961; (*d*) A. Huignard, T. Gacoin and J. P. Boilot, *Chem. Mater.*, 2000, **12**, 1090; (*e*) G. Mialon, M. Gohin, T. Gacoin and J. P. Boilot, *ACS Nano*, 2008, **2**, 2505; (*f*) Z. Hu, M. Ahrén, L. Selegard, C. Skoglund, F. Söderlind, M. Engström, X. Zhang and K. Uvdal, *Chem.–Eur. J.*, 2013, **19**, 12658; (*g*) M. Darbandi, W. Hoheisel and T. Nann, *Nanotechnology*, 2006, **17**, 4168; (*h*) Y. Sun, H. Liu, X. Wang, X. Kong and H. Zhang, *Chem. Mater.*, 2006, **18**, 2726; (*i*) G. Mialon, S. Türkcan, G. Dantelle, D. P. Collins, M. Hadjipanayi, R. A. Taylor, T. Gacoin, A. Alexandrou and J. P. Biolot, *J. Phys. Chem. C*, 2010, **114**, 22449.

10 (*a*) A. Kar, A. Datta and A. Patra, *J. Mater. Chem.*, 2010, **20**, 916; (*b*) C. Hazra, S. Sarkar, B. Meesaragandla and V. Mahalingam, *Dalton Trans.*, 2013, **42**, 11981; (*c*) Y. Wang, P. Yang, P. Ma, F. Qu, S. Gai, Y. Dai, N. Niu, F. He and J. Lin, *J. Mater. Chem. B*, 2013, **1**, 2056; (*d*) Y. Zhang, D. Geng, M. Shang, X. Zhang, X. Li, Z. Cheng, H. Lian and J. Lin, *Dalton Trans.*, 2013, **42**, 4799; (*e*) L. Perelshtein, E. Ruderman, N. Perkas, T. Tzanov, J. Beddow, E. Joyce, T. J. Mason, M. Blanes, K. Molla, A. Patlolla, A. I. Frenkel and A. Gedanken, *J. Mater. Chem. B*, 2013, **1**, 1968; (*f*) L. Perelshtein, E. Ruderman, N. Perkas, K. Traeger, T. Tzanov, J. Beddow, E. Joyce, T. J. Mason, M. Blanes, K. Molla and A. Gedanken, *J. Mater. Chem.*, 2012, **22**, 10736; (*g*) N. M. Sangeetha and F. C. J. M. van Veggel, *J. Phys. Chem. C*, 2009, **113**, 14702; (*h*) J. W. Stouwdam, M. Raudsepp and F. C. J. M. Van Veggel, *Langmuir*, 2005, **21**, 7003; (*i*) K. K. Upendra, K. Linganna, S. B. Surendra, F. Piccinelli, A. Speghini, M. Giarola, G. Mariotto and C. K. Jayasankar, *Sci. Adv. Mater.*, 2012, **4**, 584; (*j*) D. Hreniak, J. Doskocz, P. Gluchowski, R. Liciecki, W. Sterk, N. Vu, D. X. Loc, T. K. Anh, M. Bettinelli and A. Speghini, *J. Lumin.*, 2011, **131**, 473; (*k*) Y. Koltypin, S. I. Nikitenko and A. Gedanken, *J. Mater. Chem.*, 2002, **12**, 1107; (*l*) P. Jeevanandam, Y. Diamant, M. Motiei and A. Gedanken, *Phys. Chem. Chem. Phys.*, 2001, **3**, 4107.

11 C. Mazzocchia, C. Aboumrad, C. Diagne, E. Tempesti, J. M. Herrmann and G. Thomas, *Catal. Lett.*, 1991, **10**, 181.

12 D. Spassky, S. Ivanov, I. Kitaeva, V. Kolobanov, V. Mikhailin, L. Ivleva and I. Voronina, *Phys. Status Solidi C*, 2005, **2**, 65.

13 H. Barry, F. Moore and D. Robitaille, *US Pat*, 3 726 694, 1973.

14 S. S. Kim, S. Ogura, H. Ikuta, Y. Uchimoto and M. Wakihara, *Chem. Lett.*, 2001, **30**, 760.

15 R. Sundaram and K. S. Nagaraja, *Sens. Actuators, B*, 2004, **101**, 353.

16 Y. Li, G. Wang, K. Pan, Y. Qu, S. Liu and L. Feng, *Dalton Trans.*, 2013, **42**, 3366.

17 H. Wu, Y. Hu, W. Zhang, F. Kang, N. Li and G. Ju, *J. Sol-Gel Sci. Technol.*, 2012, **62**, 233.

18 A. Xie, X. Yuan, S. Hai, J. Wang, F. Wang and L. Li, *J. Phys. D: Appl. Phys.*, 2009, **42**, 105107.

19 Z. H. Zhang, Q. Huang, X. Zhao and Z. L. Huang, *Phys. Status Solidi A*, 2009, **206**, 2843.

20 X. Li, Z. Yang, L. Guan, J. Guo, Y. Wang and Q. Guo, *J. Alloys Compd.*, 2009, **478**, 686.

21 (*a*) S. I. Woo, J. S. Kim and H. K. Jun, *J. Phys. Chem. B*, 2004, **108**, 8946; (*b*) M. S. Vukasovich and J. P. G. Farr, *Polyhedron*, 1986, **5**, 559.

22 Y. S. Cho and Y. D. Huh, *Bull. Korean Chem. Soc.*, 2011, **32**, 1353.

23 Y. Tian, X. Qi, X. Wu, R. Hua and B. Chen, *J. Phys. Chem. C*, 2009, **113**, 10767.

24 Q. M. Wang and B. Wang, *Mater. Chem. Phys.*, 2005, **94**, 241.

25 X. Zhao, X. Wang, B. Chen, Q. Meng, B. Yan and W. Di, *Opt. Mater.*, 2007, **29**, 1680.

26 C. Guo, T. Chen, L. Luan, W. Zhang and D. Huang, *J. Phys. Chem. Solids*, 2008, **69**, 1905.

27 J. Wan, L. Chen, J. Sun, H. Zhong, X. Li, W. Lu, Y. Tian, H. Lin and B. Chen, *J. Alloys Compd.*, 2010, **496**, 331.

28 P. J. Gellings and H. J. M. Bouwmeester, *Catal. Today*, 1992, **12**, 105.

29 M. T. Le, M. Kovanda, V. Myslik, M. Vrnata, I. D. Van and S. Hoste, *Thin Solid Films*, 2006, **497**, 291.

30 L. T. sim, C. K. Lee and A. R. West, *J. Mater. Chem.*, 2002, **12**, 19.

31 S. Bhattacharya and A. Ghosh, *J. Appl. Phys.*, 2006, **100**, 114119.

32 (*a*) E. Cavalli, P. Boutinaud, R. Mahiou, M. Bettinelli and P. Dorenbos, *Inorg. Chem.*, 2010, **49**, 4916; (*b*) Z. Hou, R. Chai, M. Zhang, C. Zhang, P. Chong, Z. Xu, G. Li and J. Lin, *Langmuir*, 2009, **25**, 12340.

33 (*a*) G. Li, Z. Wang, Z. Quan, C. Li and J. Lin, *Cryst. Growth Des.*, 2007, **7**, 1797; (*b*) A. K. Parchur, A. I. Prasad, A. A. Ansari, S. B. Rai and R. S. Ningthoujam, *Dalton Trans.*, 2012, **41**, 11032; (*c*) B. P. Singh, A. K. Parchur, R. S. Ningthoujam, A. A. Ansari, P. Singh and S. B. Rai, *Dalton Trans.*, 2014, **43**, 4770.
34 F. Lei and B. Yan, *J. Solid State Chem.*, 2008, **181**, 855.
35 X. Li, Z. Yang, L. Guan and Q. Guo, *Mater. Lett.*, 2009, **63**, 1096.
36 (*a*) A. K. Parchur, R. S. Ningthoujam, S. B. Rai, G. C. Okram, R. A. Sing, M. Taygi, S. C. Gadkari, R. Tewari and R. K. Vatsa, *Dalton Trans.*, 2011, **40**, 7595; (*b*) A. K. Parchur and R. S. Ningthoujam, *Dalton Trans.*, 2011, **40**, 7590.
37 H. Wu, Y. Hu, W. Zhang, F. Kang, N. Li and G. Ju, *J. Sol-Gel Sci. Technol.*, 2012, **62**, 227.
38 S. Dutta, S. Som and S. K. Sharma, *Dalton Trans.*, 2013, **42**, 9654.
39 C. S. Lim, *J. Ceram. Process. Res.*, 2012, **13**, 825.
40 J. H. Chung, J. H. Ryu, S. W. Mhin, K. M. Kim and K. B. Shim, *J. Mater. Chem.*, 2012, **22**, 3997.
41 J. H. Chung, J. H. Ryu, J. W. Eun, J. H. Lee, S. Y. Lee, T. H. Heo and K. B. shim, *Mater. Chem. Phys.*, 2012, **134**, 695.
42 L. Wang, Y. Zhang and Y. Zhu, *Nano Res.*, 2010, **3**, 317.
43 W. Wang, G. K. Liu, M. G. Brik, L. Seijo and D. Shi, *Phys. Rev. B: Condens. Matter Mater. Phys.*, 2009, **80**, 155120.
44 L. Li, M. Zhao, W. Tong, X. Guan, G. Li and L. Yang, *Nanotechnology*, 2010, **21**, 195601.
45 K. Riotzki and M. Haase, *J. Phys. Chem. B*, 1998, **102**, 10129.
46 Z. Shan, Y. Wang, H. Ding and F. Huang, *J. Mol. Catal. A: Chem.*, 2009, **302**, 54.
47 M. Shen, Q. Zhang, H. Chen and T. Peng, *CrystEngComm*, 2011, **13**, 2785.
48 Q. I. Rahman, M. Ahmad, S. K. Misra and M. Lohani, *Mater. Lett.*, 2013, **91**, 170.